J. of Korean Ind. & Eng. Chemistry,
Vol.4, No.1, March 1993, 153-161

Cathodic Polarization Measurements on $La_{0.9}Sr_{0.1}MnO_3$ Electrode for Solid Oxide Fuel Cells

H. Y. Lee and S. M. Oh

Department of Chemical Technology, College of Engineering
Seoul National University, Seoul, 151-742, Korea
(*Received August 11, 1992, Accepted November 9, 1992*)

Abstract: Cathodic oxygen reduction kinetics on $La_{0.9}Sr_{0.1}MnO_3$ electrode have been examined at 700-900℃ under various oxygen partial pressures. AC impedance and current interruption techniques were employed for the determination of charge transfer resistances for electrochemical oxygen reduction. The R_{ct} values obtained from two different methods were very close each other for $La_{0.9}Sr_{0.1}MnO_3$ electrode. Activation energy for the electrochemical oxygen reduction was found to be 174kJ/mol under atmospheric oxygen pressure. R_{ct} measurements as a function of oxygen partial pressure indicate that the rate-determining step for the electrochemical oxygen reduction on $La_{0.9}Sr_{0.1}MnO_3$ electrode is the charge transfer process.

요 약 : 700-900℃의 온도범위와 여러 산소분압 조건에서 고체전해질 연료전지의 양극인 $La_{0.9}Sr_{0.1}MnO_3$에서 산소의 환원반응특성을 조사하였다. AC 임피던스법과 전류중단법에 의해 산소환원반응의 전하전달저항을 측정하였는데 두 방법으로 구한 값이 서로 잘 일치하였다. 전기화학적 산소환원반응의 활성화에너지는 대기압 조건에서 174kJ/mol의 값을 보였고, 산소분압에 따른 전하전달저항의 측정결과로 부터 이 전극에서 전기화학적 산소환원반응의 율속단계는 전하전달과정임을 알 수 있었다.

1. Introduction

Recently, there has been a cosiderable interest in solid oxide fuel cell systems[1, 2]. The solid oxide fuel cell (SOFC) is an all solid-state power generation system, which operates at hgih temperatures to ensure adequate ionic and electronic conductivity of its component materials. Because of its high operating temperature, activation overpotentials are generally low and noble metal electrocatalysts are not necessary. Also, the system can provide for internal reforming of natural gas and other hydrocarbons to produce CO and H_2, for which is even more effective than in lower temperature fuel cell systems. Furthermore, high temperature waste heats can be used for other power generation systems or heating utilities. However, the high operating temperature leads to severe materials problems for the electrodes and electrolytes. Chemical stability at an oxidizing and reducing atmosphere, phase stability at high operating temperatures, interfacial stability between electrode and electolyte, compatability in thermal expansion coefficients between the component materials are the stringent requirements for successful devices.

As to the air electrodes, selection of electrode materials with low activation overpotential and their fabrication techniques with adequate morphology

are another important subjects in addition to the above-mentioned requirements. A variety of materials have been proposed for cathodes. However, perovskite oxides seem to be the most promising for the SOFCs[3-9]. Perovskite oxides, $La_{1-x}Sr_xMO_3$(M =Mn, Fe, Co), which are widely used in the present day SOFCs, have been proposed to be an electronic conductor, but under high cathodic polarization conditions they become partially reduced, creating oxide vacancies, hence mixed-conduction. Several previous investigations have shown the favorable influence of a high Sr dopant concentrations on the electrochemical activity for oxygen reduction[6-8]. Such a high catalytic activity is often discussed in terms of oxygen nonstoichiometry, more precisely in terms of an additional ionic conductivity responsible for the broadening of the effective electrode reaction zone. It allows direct electronic charge transfer reactions with oxygen at all surface sites of the mixed-conducting electrodes and does not require surface diffusion of adsorbed oxygen. This was assumed to lead to principal advantages as compared to the charge transfer mechanisms with noble metal electrodes requiring surface diffusion to the three phase boundary sites. Some results[9, 10], however, indicate that the electrode kinetics at perovskite electrodes are not exclusively determined by the diffusion kinetics of oxide ions in the bulk of the electrodes. The surface processes including the surface diffusion of oxygen atoms seem to be more important for their contribution to the overall kinetics than assumed before. This is one of the critical issues to be clarified in the research of SOFCs.

Another unsolved subject in the research field of SOFCs is the oxygen reduction kinetics on cathodes [11-16]. The oxygen reduction on cathodes has several elementary steps and almost all the possible processes have been proposed as the rate-controlling step of the overall reaction; gaseous oxygen diffusion within the pores of the electrode, adsorption of oxygen on the electrode, diffusion of dissolved oxygen through the electrode, and charge transfer reaction. It is believed that the contradictions are partially come from the difference in morphology of the electrodes and the methods of data analysis. Thus, for a precise analysis of the cathoic reaction kinetics, relationship between the electrochemical activity and the microstructures of the electrodes should be investigated. Also a general theory and experimental techniques are needed for the resolution of the above contradictions, offering a logical explanation to all of the data.

The principal purpose of this study is the examination of oxygen reduction kinetics on a perovskite electrode, $La_{0.9}Sr_{0.1}MnO_3$. AC impedance and current interruption methods have been utilized for the study of reaction kinetics and self-consistent results have been obtained. During the work, experimental techniques for the characterization of electrode kinetics have been established. Also, the nature of the rate-controlling step for the electrochemical oxygen reduction on $La_{0.9}Sr_{0.1}MnO_3$ electrode has been identified.

2. Experimentals

2. 1. Materials

$La_{0.9}Sr_{0.1}MnO_3$ powder was synthesized by the citrate method. Aqueous solutions of nitrate of La, Sr, and Mn were mixed together in a proper molar ratio, into which the equivalent amount of citric acid was added. The resulting solutions were then concentrated to have viscous sols and further dried under vacuum to have gels. The gels were crushed and heat-treated on the heating schedule as represented in Fig. 1. The heating schedule was turned out to be important factor to have single perovskite phase. Other phases except the perovskite were not found in the XRD powder patterns in the specimens treated with the proper heating schedule. Fig. 2. represents the XRD pattern for the perovskite oxide powder, which is consistent with the reported data [17]. The calcined powders were washed with distilled water and dried at 110℃. The final powder specimens were obtained after screening with 400 mesh standard sieve.

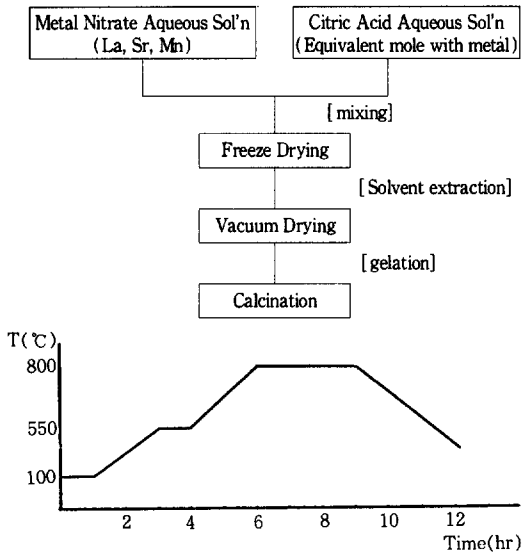

Fig. 1. Schematic diagram for the powder Preparation and the heating schedule.

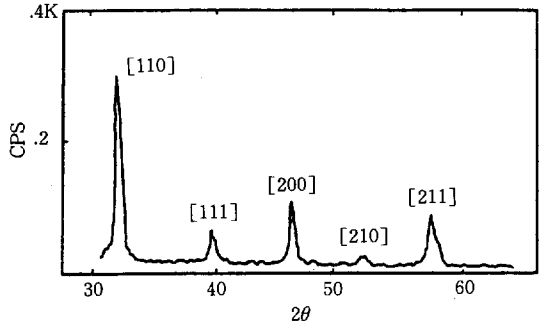

Fig. 2. XRD pattern for the $La_{0.9}Sr_{0.1}MnO_3$ powder.

2. 2. Preparation of Electrodes

The electrode layers were prepared by slurry-coating technique. The mixture of oxide powder, solvent, binder, plasticizer, and homogenizer were ball-milled and treated with ultrasonic vibrator in order to prevent agglomeration. The composition of the slurry is listed in Table 1. The slurries were painted on 8 mol% Yttria-stabilized Zirconia(YSZ) disk (Koshin Products, diameter=25mm, thickness=1mm) and calcined at 1200℃ for 6 hrs. As counter and reference electrodes, Pt paste(Ferro Corp., 4082) was painted and 100 mesh Pt gauze was attached on the other side of the disk as shown in Fig. 3. SEM observation of the electrode layer(see Fig. 4) indicates that the electrode layer has desirable porosity and the thickness is about 4μm.

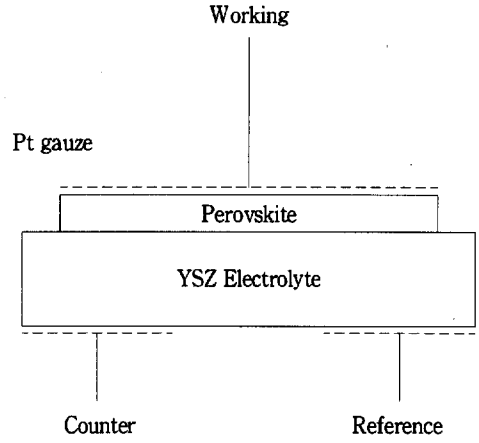

Fig. 3. Schematic diagram of the Experimental Cell.

Table 1. The Composition of Sluries(vol %)

powder	perovskite oxide	35
sovent	ethyl alcohol	20
	methylethylketone	14
binder	polymethylmethacrylate	20
plasticizer	polyethyleneglycol(# 400)	10
homogenizer	cyclohexanone	1

2. 3. Electrochemical Measurements

Electrochemical measurements were carried out with the three electrode configuration as depicted in Fig 3. Only half-cell characteristics of the cathode were measured under various oxygen pressures at 700-900℃. The partial pressure of oxygen was controlled by mixing the proper ratio of N_2 and O_2, and the actual oxygen pressure was measured by zirconia-based oxygen sensors. AC impedance measurements were made over the frequency range of 0.05Hz-100KHz using EG & G PARC 173 Potentiostat/Galvanostat, 276 Interface, and 5208 Two Phase Lock-in Analyzer. Steady-state cathodic polarization was measured by the current interruption method using EG & G PARC Potentiostat/Galvanostat, 175 Function Generator, and a personal computer connected by EG & G PARC 276 In-

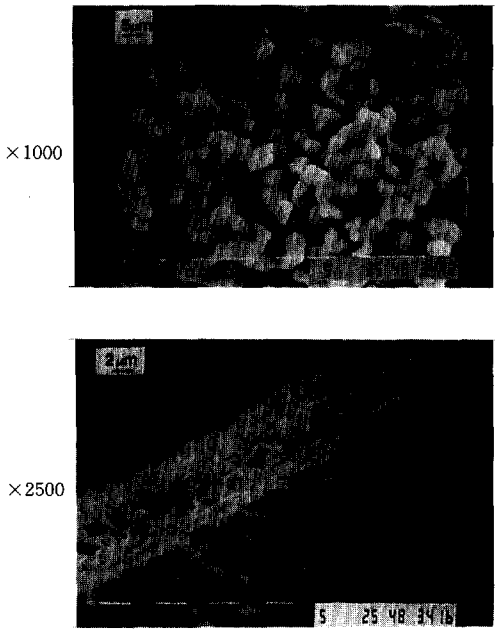

Fig. 4. SEM photographs of the perovskite oxide electrode.
Top; Top view showing the prosity of the electrode
Bottom; Side view showing the thickness of the electode layer

terface. Deconvolution of the complex impedance spectra was performed with EG & G PARC 378 Electrochemical Impedance Software.

3. Result and Discussion

3. 1. AC Impedance Analysis

The present cell configuration can be accounted for with the equivalent circuit as depicted in Fig 5, where R is a resistor, C is a capacitor and CPE is the constant phase element. The CPE may be expressed by $Z_0(j\omega)^{-n}$ and can be reduced to a capacitor, resistor, inductor, and a Warburg diffusional element when n takes the values of 1, 0, -1, and 0.5, respectively[18]. The components of the equivalent circuit in Fig. 5 may be assigned to different processes taking place in the system; the R_{el} is the electrolyte resistance between the working and reference electrode, R_{gb} and C_{gb} correspond to the grain boundary resistance and capacitance, R_{ct} to the charge transfer resistance for oxygen reduction.

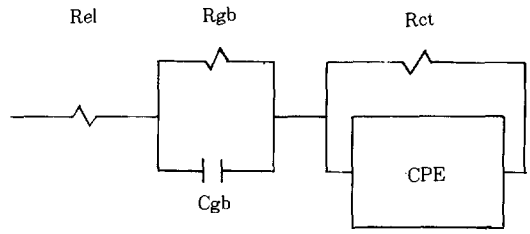

Fig. 5. The equivalent circuit for the experimental cell configuration.
R_{el} ; electrolyte resistance
R_{gb} ; grain boundary resistance
C_{gb} ; grain boundary capacitance
R_{ct} ; charge transfer resistance
CPE ; constant phase element

Typical complex impedance spectra are plotted in Fig. 6. The spectra show only one semicircle with a time constant of about 1 sec. This indicates that semicircle related with the grain boundary component is absent, that is, the R_{gb} and C_{gb} have negligibly small values. It has been reported[19] that time constants for the parallel combination of grain boundary resistance and capacitance are about 1 msec. Thus, the equivalent circuit in Fig. 5 can be simplified as the sum of R_{el} and the parallel combination of R_{ct} and CPE. Also, the spectra in Fig. 6 illustrate that the impedance arcs are slightly de-

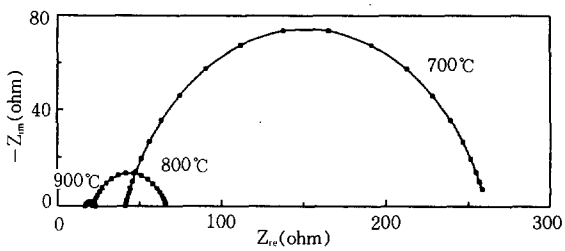

Fig. 6. The complex impedance plots for the electrochemical oxygen reduction on $La_{0.9}Sr_{0.1}MnO_3$ /YSZ/Pt in air.

pressed and this depression becomes significant as the measuring temperature increases. This manifests itself that the cell configuration is expressed not only by the single RC parallel circuit but also by the small additional contribution of the Warburg type diffusional term. The diffusional term becomes significant as the temperature is increased. This result supports the suggestions[20, 21] that the rate-controlling step for the oxygen reduction reaction be the charge transfer step at lower temperatures but the oxygen diffusion becomes more important at higher temperature range.

Typical temperature-dependent impedance spectra are demonstrated in Fig 6. As can be seen in the figure, the R_{el} and the radii of the semicircles, that is, the R_{ct} values become smaller as the measuring temperature is raised. This can be easily understood with the fact that both the oxide ion conductivity in YSZ electrolyte and the charge transfer rates at the electrodes are increasing as proportional to the temperature. The R_{ct} values were obtained by deconvoluting the spectra by the non-linear least square method and listed in Table 2 along with the values obained by the current interruption method.

Table 2. Charge Transfer Resistance(R_{ct}) Values Measured in Air(P_{o2}=0.21atm)

T(℃)	700	750	800	850	900
R_{ct}	220.4	97.5	45.2	18.3	6.2
(Ω)	219.2	95.3	48.7	16.4	6.4

The numbers at the top correspond to the R_{ct} values measured by AC Impedance technique and the bottom ones to those measured by the current interruption method.

3.2. Polarization Measurement by Current Interruption Method

Steady-state polarization behaviors of the electrodes were investigated with the current interruption method[22]. The equivalent circuit for the present cell configuration can be simplified as shown in the inset of Fig. 7, ignoring the grain boundary component and assuming the CPE element to be a simple capacitor. The top figure represents the

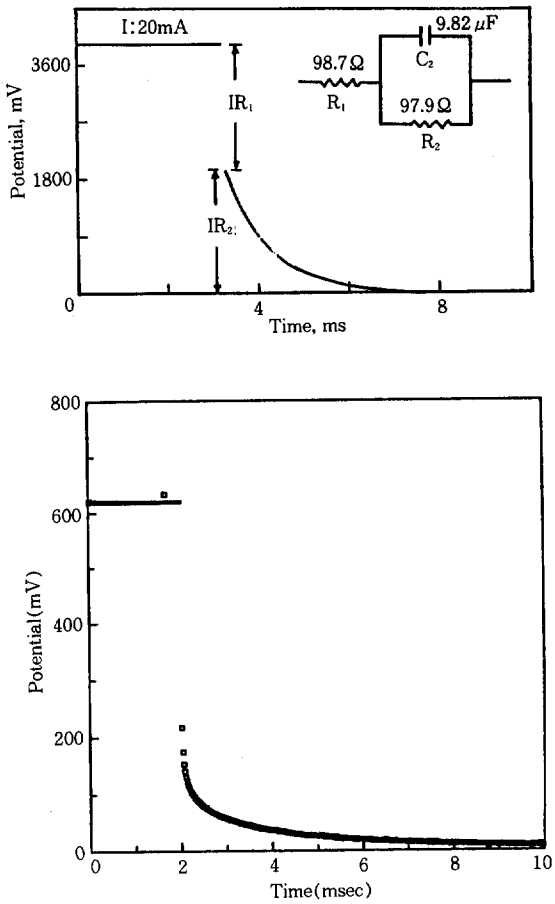

Fig. 7. Typical potential decay patterns during the current interruption.
To; simulated decay pattern with a dummy cell illustrated in the inset.
Bottom; observed decay pattern with $La_{0.9}Sr_{0.1}MnO_3$ at 800℃ in air(I=20.8mA/cm^2)

potential vs. time profile during a current interruption, which is a simulated profile with a dummy cell represented in the inset. The measured potential decay plot, obtained with $La_{0.9}Sr_{0.1}MnO_3$ at 800℃ in air, is presented at the bottom of Fig 7. The simulated and observed traces look similar. The overpotential values for oxygen reduction were obtained from the exponentially decayed portion in the decay pattern.

The cathodic polarization characteristics for the perovskite electrode in air were plotted in Fig 8, which represents the measured overpotentials at the imposed current densities. The R_{ct} values were calculated from the current and overpotential values within the small overpotential range where Butler-Volmer equation can be applied. The temperature-dependent R_{ct} values were listed in Table 2. The numbers obtained from two different methods are very close each other. Also it can be seen that the R_{ct} values become smaller as the measuring temperature is increased.

3. 3. Activation Energy for the Charge Transfer

The exchange current densities were calculated from the measured R_{ct} values according to the following equation.

$$I_0=\frac{RT}{nF\,R_{ct}} \qquad (1)$$

The temperature-dependent exchange current density under atmospheric oxygen pressure was plotted in Fig. 9. From this plot, the activation energy for the charge transfer reaction was calculated to be 174kJ/mol, E_A values have been reported for other electrode materials; 100kJ/mol for Pt paste electrode/CeO_2[12], 180kJ/mol for $La_{0.7}Sr_{0.3}MnO_3$ [3, 4], and 60kJ/mol for $La_{0.6}Sr_{0.4}MnO_3$[15]. Our result is very close to the value obtained by Takeda et al[3, 4]. However, as described later, they proposed that diffusional processes of molecular or atomic oxygens be the rate-controlling step for oxygen reduction. Our results indicate that the rate-limiting step is the charge transfer process(see the next section). It is likely that the two numbers are fortuitous since E_A values should generally be different if disparate rate-limiting processes are involved. Sometimes, measured E_A value can give us a clue on the rate-limiting process for overall kinetics. Unfortunately, relevant reported results on E_A values and the nature of the rate-limiting process for perovskite electrodes are not enough for us to compare with.

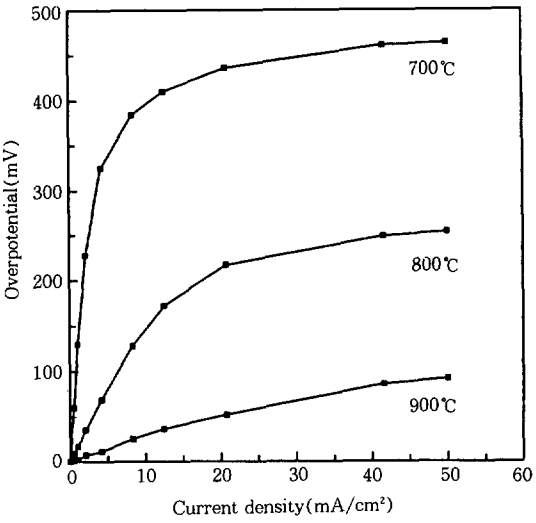

Fig. 8. The cathodic polarizations for the $La_{0.9}Sr_{0.1}MnO_3$ electrode in air.

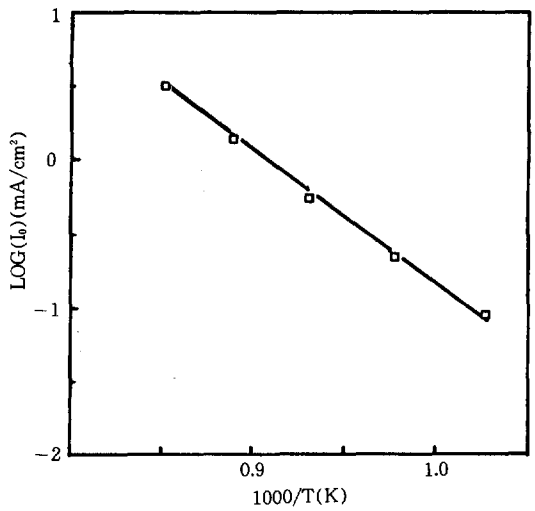

Fig. 9. The arrhenius plot for the determination of activation energy for the electrochemical oxygen reduction.

3. 4. Oxygen Reduction kinetics

In order to identify the nature of the rate-controlling process for oxygen reduction reaction, R_{ct} values were measured according to the oxygen partial pressure. Fig. 10 and 11 demonstrate the results, where the complex impedance spectra were potted

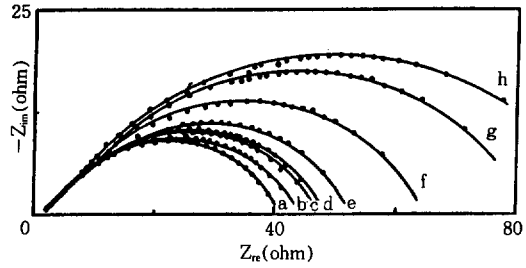

Fig. 10. The complex impedance plots under different oxygen pressure at 800℃. a; 0.647atm, b; 0.502atm, c; 0.361atm, d; 0.3atm, e; 0.184atm, f; 0.095atm, g; 0.037atm, and h; 0.025atm.

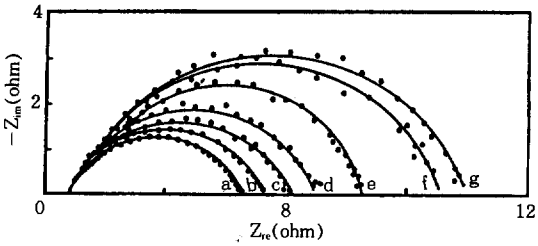

Fig. 11. The complex impedance plots under different oxygen pressure at 900℃. a; 0.621atm, b; 0.388atm, c; 0.3atm, d; 0.165atm, e; 0.099atem, f; 0.036atm, ant g; 0.025atm.

as a function of oxygen partial pressure at 800℃ and 900℃. As can be seen in the figures, the R_{ct} values become larger as the Po_2 decreases. The log I_0 vs. log Po_2 plots are preseted in Fig 12. The slopes in the plot are very close to 1/4.

It has generally been accepted that oxygen reduction on perovskite oxides takes place along the following consecutive reaction steps[12, 14].

$$O_2(gas)=O_2(ads) \quad \text{(oxygen diffusion)} \quad (2)$$
$$O_2(ads)=2O(ads) \quad \text{(dissociative adsorption)} \quad (3)$$
$$O(ads)+2\acute{e}+V\ddot{o}=O\ddot{o} \quad \text{(charge transfer)} \quad (4)$$

where $V\ddot{o}$ and $O\ddot{o}$ are the vacant and occupied surface oxygen sites, in Kröger-Vink notation, respectively. The slowest step would determine the overall reaction rate, that is, reduction current. According to Wang and Nowick[12, 14], the exchange

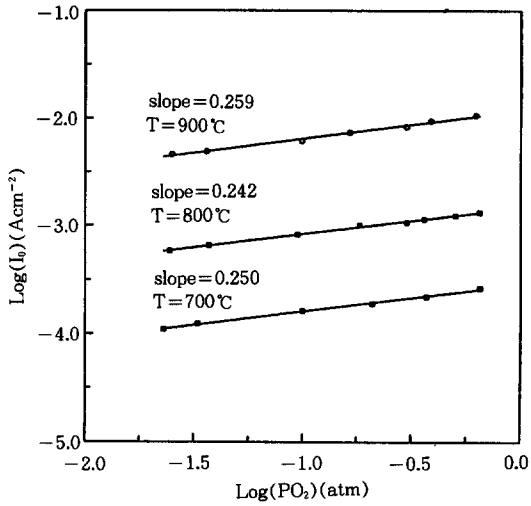

Fig. 12 The log I_0 vs. log Po_2 plots for the $La_{0.9}Sr_{0.1}MnO_3$ electrode.

current density can be expressed as a function of oxygen partial pressure.

$$I_0 \propto (Po_2)^n \quad (5)$$

and the n values have 1 if the rate-limiting step is diffusional process of molecular oxygen, 1/2 for dissociative adsorption and ± 1/4 for charge transfer process depending on the conditions for Langmuir adsorption isotherm. That is, from the mass action law of the adsorption step based on the Langmuir isotherm, Po_2 is related as

$$\frac{\theta}{1-\theta}=(K_{ad} \cdot Po_2)^{1/2} \quad (6)$$

where θ is the fraction of adsorption sites occupied by oxygen atoms and K_{ad} is the equilibrium constant. The rate of reaction corresponds to the exchange current density

$$I_0 = nFk_r[\theta(1-\theta)]^{1/2} \quad (7)$$

where n is the charges transferred in the rate-determining step, F is the Faraday constant and k_r is the reaction rate constant. At very small coverage($\theta \cong 0$), which is valid for $K_{ad} \cdot Po_2 \ll 1$, and thus at high temperatures and/or low Po_2, the exchange current

density can be expressed as

$$I_0 = nFk_r(K_{ad} \cdot P_{O_2})^{1/4} \quad (8)$$

However, for the fully covered surface($\theta \cong 1$), which corresponds to $K_{ad} \cdot P_{O_2} \gg 1$, and thus at low temperatures and/or high P_{O_2},

$$I_0 = nFk_r(K_{ad} \cdot P_{O_2})^{-1/4} \quad (9)$$

Thus, the slope of log I_0 vs. log P_{O_2} plots become 1/4 or -1/4 depending on the condition of the Langmuir isotherm for the charge transfer limiting condition.

In this study for $La_{0.9}Sr_{0.1}MnO_3$, the slopes in the log I_0 vs log P_{O_2} were turned out to be 1/4 at 700-900℃. This indicates that the rate-limiting step for the electrochemical oxygen reduction in this temperature range is the charge transfer process. Also it can be seen that the present experimental conditions are located within the high temperature and/or low P_{O_2} regime, assuming the Langmuir adsorption isotherm is prevailing.

Takeda et al.[4] carried out the similar experiment on $La_{1-x}Sr_xMnO_3$($x=0.3$-0.7). They found, however, that the n values were close to 3/4, suggesting that combination of the molecular oxygen diffusion and the dissociative adsorption is rate-limiting.

4. Summary and Comment

In this study, experimental techniques have been established for the characterization of polarization behaviors of oxygen reduction on cathodes. The charge transfer resistance values obtained from the AC impedance and current interruption techniques are very close each other. The E_A value for the electrochemical oxygen reduction in air was calculated to be 174kJ/mol. Also, it has been suggested that the rate-determining step for oxygen reduction be the charge transfer process on this electrode.

However, further experimental works are still needed for full understandings of the electrode kinetics on perovskite electrodes, that is, the nature of the active sites for oxygen reduction reaction and the issues of effective area expansion in perovskite electrodes. To this end, exchange current density and oxygen nonstoichiometry in perovskite oxides should be correlated each other. If the charge transfer reaction takes place at the whole area of the oxide and perovskite oxides have additional ionic conductivity responsible for the broadening of effective electrode reaction zone, higher activity for oxygen reduction would be expected in the perovskite oxides containing larger amount of oxide vacancies [6-8]. On the other hand, if the three-phase boundaries are active for oxygen reduction, electrode kinetics would rather be dependent on the degree of adhesion at the electrolyte/electrode interface and the effective area of the three phase boundaries. These works are under going in this laboratory.

Acknowledgement

This work was supported by a grant from the Ministry of Energy and Resources, Korea.

REFERENCES

1. W. Göpel and H. D. Wiemhöfer, *Ber. Bunsenges. Phys. Chem.*, **94**, 981(1990).
2. A. Hammou, *Proc. Inter. Seminar on Solid State Ionic Devices, Singapore*, 1988, pp.243-263.
3. O. Yamamoto, Y. Takeda, R. Kanno, and M. Noda, *Solid State Ionics*, **22**, 241(1987).
4. Y. Takeda, R. Kanno, M. Noda, Y. Tomida, and O. Yamamoto, *J. Electrochem. Soc.*, **134**, 2656 (1987).
5. B. C. H. Steele, I. E. Kelly, P. H. Middleton, and R. A., Rudkin, *Solid State Ionics*, **28-30**, 1547 (1988).
6. A. Hammouche, E. Siebert, and A. Hammou, *Mat. Res. Bull.*, **24**, 367(1989).
7. T. Kenjo, Y. Horiuchi, and S. Osawa, *J. Electrochem. Soc.*, **137**, 24243(1990).
8. A. Hammouche, E. Siebert, A. Hammou, and M. Kleitz, *ibid.*, **138**, 1212(1991).

9. J. Mizusaki and H. Tagawa, *Proc. Intern. Symposium on SOFCs, Nagoya*, (1989).
10. J. Mizausaki, H. Tagawa, K. Tsuneyoshi, and A. Sawata, *J. Electrochem. Soc.*, **138**, 1867 (1991).
11. P. Fabry and M. Kleitz, *J. Electroanal. Chem.*, **57**, 165(1974).
12. D. Y. Wang and A. S. Nowick, *J. Electrochem. Soc.*, **126**, 1155(1979).
13. B. L. Kuzin and M. A. Komarov, *Solid State Ionics*, **39**, 163(1990).
14. D. Y. Wang, *ibid.*, **40–41**, 849(1990).
15. T. Inoue, N. Seki, K. Eguchi, and H. Arai, *J. Electrochem. Soc.*, **137**, 2523(1990).
16. O. J. Velle, T. Norby, and P. Kofstad, *Solid State Ionics*, **47**, 161(1991).
17. Y. Ohno, S. Nagata, and H. Sato, *Solid State Ionics*, **9–10**, 1001(1983).
18. I. D. Raistrick, J. R. MacDonald, D. R. Franceschetti, in "Impedance Spectroscopy", ed., J. R. MacDonald, Wiely & Sons, New York, (1987), chap 2.
19. J. E. Bauerle, *J. Phys. Chem. solids*, **30**, 2657 (1969).
20. J. Sasaki, J. Mizusaki, S. Yamauchi, and K. Fueki, *Bull., Chem. Soc. Japan*, **54** 1688(1981).
21. T. Inoue, K. Eguchi, T. Setoguchi, and H. Arai, *Solid State Ionics*, **40–41**, 407(1990).
22. A. E. Hughes and S. P. S. Badwal, *ibid.*, **40–41**, 312(1990).